

# Variable Line Profiles Due to Non-Axisymmetric Patterns in an Accretion Disc around a Rotating Black Hole<sup>1</sup>

Vladimír Karas, Andrea Martocchia<sup>y,z</sup> and Ladislav Šubr

Astronomical Institute, Charles University Prague, V Holesovickách 2, CZ-180 00 Praha, Czech Republic

<sup>y</sup> Scuola Internazionale Superiore di Studi Avanzati, Via Beirut 2-4, I-34014 Trieste, Italy

<sup>z</sup> Terza Università degli studi di Roma, Dipartimento di Fisica, Via della Vasca Navale 84, I-00146 Roma, Italy

vladimir.karas@m.cuni.cz, martoc@haendel.suniroma3.it, subr@agla.jam.s.m.cuni.cz

(Received 2000 December 19; accepted 2001 January 29)

## Abstract

We have explored spectral line profiles due to spiral patterns in accretion discs around black holes. A parametrization was employed for the shape and emissivity of spiral waves, which can be produced by non-axisymmetric perturbations affecting the disc density and ionization structure. The effects of the light-travel time, energy shift, and gravitational focusing near to a rotating black hole were taken into account. A high-resolution ray-tracing code was used to follow the time variations of the synthetic line profile. A variety of expected spectral features were examined and the scheme applied to a broad iron line observed in MCG +6-30-15.

**Key words:** accretion, accretion disks { black hole physics { galaxies: nuclei { galaxies: individual (MCG +6-30-15) { X-rays: galaxies

## 1. Introduction

Time-dependent phenomena are of extreme richness, variety, and observational relevance for accreting black-hole systems (e.g., Kato et al. 1998; Krolik 1999). Clearly, astrophysically realistic processes must result from the interplay of different factors which affect light-curves and produce spectral features. Here we concentrate on the X-ray spectral band.

Rapid temporal changes of the flux and of individual spectral features are observed in many active galactic nuclei (AGN) and in Galactic black-hole candidates (GBHCs). Variability patterns fit well with the widely adopted scenario of these objects as massive black holes surrounded by accretion flows, in the form of a disc or a torus (e.g., Ulrich et al. 1997). The X-ray variability of AGN and of GBHCs is often attributed to instabilities in their accretion flows causing changes in the inner and outer boundaries of the radiating disc region or relatively persistent non-axisymmetric inhomogeneities in the disc itself. This paper deals with variability properties which can be due to spiral structures forming in the inner part of the disc at distances  $< 100r_g$  from the centre. We consider rotating (Kerr) black holes together with spiral waves of density perturbation in the disc matter. The

waves are supposed to modify the emissivity pattern of the gaseous flow.

A power-law continuum is observed in X-ray spectra, which is thought to provide primary irradiation of the flow. Numerical computations of local reflection spectra from X-ray irradiated material suggest that the emissivity depends strongly on the nature and location of the primary source (e.g., Martocchia & Matt 1996; Martocchia 2000, and references therein), and also on the ionization structure and density profile of the flow (Done, Nayakshin 2001). Only in the case of density larger than a critical value and small ionization parameter, the matter behaves like a pure optically thick medium from which a typical cold iron line is emitted (Nayakshin et al. 2000; Dumont et al. 2000). The extent to which ionization in the disc influences emission and absorption features is subject of much debate.

As far as the power-law continuum is concerned, a plausible scheme suggests that this spectral component is produced in a hot Comptonizing medium (corona) above the disc. Another possibility is that magnetic reconnection causes temporary, strong flashes of radiation (ares) near the inflowing matter (Galeev et al. 1979; Coppi 1992; Hårdt et al. 1994; Nayakshin 1998). Several mechanisms have been proposed for ares, but the available spectroscopy does not allow us to decide among them; see Malzac and Jourdain (2000) for recent discussion and

<sup>1</sup> Low-resolution figures have been used in order to conform to the standards of astro-ph e-print library.

further references. The flares are supposed to irradiate the gas in their neighbourhood, contributing to short-term variability (Minoshige et al. 1994; Yonehara et al. 1997). Furthermore, the coronal activity may be localized in asymmetric and rapidly evolving areas. In both cases (flares vs. inhomogeneous coronal activity) variations in the primary flux are expected, which also determine the variation in the additional spectral features due to Compton reflection (a continuum "hump") and fluorescence (lines).

In this work we explored the expected spectral line profiles in the region where relativistic light-travel time, energy shift and lensing effects influence substantially the observed radiation fluxes, temporal variability, and the lines centroid energy. We assumed that a perturbation (of density and ionization structure) develops on length-scales of ten or a few tens of gravitational radii, giving rise to emissivity contrast against the background of the axisymmetric flow. The spirals become active after being illuminated from the primary source. Here, one has to distinguish between two cases: (i) the primary illumination independent from the origin of the spiral perturbation of the disc; (ii) the two phenomena (the disc perturbation and the flare) being connected to each other. The second case is particularly relevant for binary systems with Roche-lobe overflow; in such a situation, the outer end of the spiral pattern coincides with the place where the overflowing material hits the disc. This is the place where a flare or a spot develops. Therefore, we consider the emissivity variations with simultaneous contributions from the spiral pattern and from the flare.

We computed the predicted, variable line profiles with the aim of assessing the importance of the mentioned effects, especially the degree of the line flux and energy fluctuations that could be assigned to the existence of such non-axial structures. We also mention our computational approach, which can be adapted to different intrinsic emissivities and the source geometry, and, for the sake of illustration, we determine free parameters of the phenomenological model for the variable iron K emission of the Seyfert galaxy MCG 6-30-15.

Rapid variations have been reported in the X-ray continuum and in the K iron line of MCG 6-30-15 (6.7 keV), namely, Iwasawa et al. (1996, 1999) described the spectral changes which occurred during ASCA observations in 1994 and 1997. It is important to examine how the changes of selected spectral features – and the fluorescent iron feature in particular – reflect the changes in primary illumination, because this helps to constrain the geometry of the emitting regions, for instance by reverberation techniques (Reynolds et al. 1999; for a recent review, see Fabian et al. 2000).

We start the next section by giving some further hints on the physical models which justify our interest in considering the spiral-type patterns.

## 2. The Model

In AGN, variability time-scales go down to less than one hour, which is almost comparable with the light-crossing time ( $t_c$ ) at distances of the order of the gravitational radius ( $r_g$ ) of a supermassive black hole:  $t_c \approx 10^2 M^{-1} s$ , where  $M$  is the central mass in units of  $10^7 M_\odot$ . Other time-scales relevant to black-hole accretion discs (orbital, thermal, sound-crossing, and viscous) are typically longer than  $t_c$ . Characteristic time-scales of the observed variability also depend on the inclination of the system with respect to an observer, and can be scaled with the mass of the central object. Moreover, time intervals become longer very near to the hole if gravitational delays predicted by general relativity are taken into consideration.

### 2.1. Astrophysical Motivations

The irradiation of the disc from a varying source of primary X-rays does not lead to instantaneous response, but generates reflection or fluorescence. A delay occurs depending on the geometrical and physical state of the gaseous material. For example, Blandford and McKee (1982) and Taylor (1996) have discussed the intrinsic delays of the response in the case of clouds geometry, but here such effects are not considered for simplicity. Instead, it is the location of the primary source – often identified in one or more arcing regions – together with reflection patterns in the disc which determine the observed signal. A single variability event is therefore made of a primary flare and a complex response due to Compton reflection (or fluorescence, in the case of the iron line) by the disc matter at various distances from the hole.

Several people have considered the reprocessing of primary X-rays recently (for references, see Dumont et al. 2000; Karas et al. 2000; Nayakshin et al. 2000). Reprocessed radiation reaches the observer from different regions of the system. Individual rays experience unequal time lags of – but for purely geometrical reasons, and other relativistic effects occur in the very vicinity of the hole and are relevant for the source variability, namely, lensing and Doppler boosting (Rauch, Blandford 1994). In the case of long-lived patterns ( $t \gg t_c$ ) in the disc, there is, indeed, a substantial contribution to the variability caused by the orbital motion (Abramowicz et al. 1991; Mangalam, Wita 1993). If the disc is strictly equatorial, two types of such patterns have been examined in more detail: spots (which could be identified with vortices in gaseous discs; cf. Abramowicz et al. 1992; Adams, Watkins 1995; Karas 1997), and spiral waves. In principle it is possible to distinguish different origins of the varying emission, namely, short-lived flares which decay on the dynamical time-scale versus long-duration features (Lawrence, Papadakis 1993; Kawaguchi et al. 2000). To that purpose, the geometry of the system needs to be con-

strained sufficiently. In addition to intrinsic variations, obscuration is involved along the path of light rays towards the observer. The light propagation is affected by the presence of refractive interstellar medium on the line of sight (Rickett et al. 1984) which contributes, together with internal and random obscuration, to rapid and high-amplitude flickering seen by the distant observer (Abrassart, Czerny 2000). These non-intrinsic effects are beyond the scope of this paper.

The spiral waves represent large-scale structures (size comparable with the radius), which can be induced by non-axisymmetric perturbations (Sanders, Huntley 1976; Wada 1994; Lee, Goodman 2000) or due to magnetic instabilities (Tagger et al. 1990). Also, a pattern resembling a single-armed spiral is produced from an extended spot after its decay due to shear motion in the differentially rotating disc. Even though such a pattern is only a transient feature, it may last sufficiently long to produce observable effects. Thus, the spirals are expected to arise naturally in accretion discs and to persist there for times longer than the orbital period of the flow particles. Sanders, Huntley (1976) demonstrated that the formation of a two-arm spiral wave is a natural response of differentially rotating gaseous discs to an oval gravitational perturbation, much like in the case of a self-gravitating stellar system into which the gas is assumed to be embedded. Recently, Kuo and Yuan (1999) examined the excitation of spiral waves in Lindblad resonances by comparing the asymptotic theory of bar-driven waves with the corresponding results of numerical computations. In a different way, Tagger and Pellat (1999) showed that spirals can be formed due to a certain kind of magnetic instability; such waves remain localized close to the inner radius of the disc. In general, spiral patterns can develop an odd or even number of arms depending on the type of the perturbing forces that act on the disc.

Spiral patterns have been treated in the theory of stellar systems, and widely discussed in the context of non-axisymmetric perturbations which can modify density profiles and emissivities of gas discs (Goldreich, Tremaine 1979; Sawada et al. 1986; Rozyczka, Spruit 1993). The status of SPH computations was summarized recently by Lanzafame, Maravigna and Belvedere (2000) who examined the role of stellar-mass ratio on the formation of spiral structures in binaries. The spirals meet numerous applications also with respect to cataclysmic variables (Steehls, Stehle 1999). Furthermore, the modulation of X-rays by spiral waves was also proposed with regard to polars (Murray et al. 1999).

Most of the attention with regard to spiral waves spectral features has been motivated by studies of cataclysmic variables and other stellar-mass binary systems. It was noted that the variation in the density profile and ionization of accretion flows, predicted by numerical and semi-analytical methods, is followed by temperature modu-



Fig. 1. Geometry of the model: an artistic expression of spiral patterns in an accretion disc. In the present work, the intrinsic emissivity is described by a small number of free parameters which also determine the variability of the spectral features. We consider the emissivity to be modulated by the spiral pattern with an associated decaying core.

lation, and therefore by a change in the gas (thermal) emissivity within the spiral patterns. A similar effect is also expected for the X-ray irradiated accretion flows in AGN due to an increase in the matter density along the patterns (if optical thickness  $< 1$ ) or variations in the ionization structure (the emissivity is not sensitive to density changes if  $> 1$ ). A phenomenological description appears to be adequate for the current scenario of X-rays reprocessing in AGN cores, and is convenient for the numerical computation of line profiles.

As far as AGNs are concerned, spiral waves have been explored as possible sources of spectral line variations in the context of broad emission-line regions (Chen, Halpern 1990; Chakrabarti, Wilita 1993, 1994; Eracleous 1998) and in maser sources (Maoz, McKee 1998). In these studies, because the radiation originates at distances  $> 10^3 r_g$  from the centre, general-relativity effects are unimportant and variability time-scales are of the order of several months to years. On the other hand, Sanbuchi, Fukue and Kojima (1994) considered spirals extending close to a Schwarzschild black hole where the effects of general relativity play a role, and showed examples of relativistically distorted spectra.

## 2.2. A Toy Model of Spiral-Wave Emissivity

We parametrize the Kerr spacetime in terms of the black hole specific angular momentum ( $0 \leq a \leq 1$ ). In the disc plane, we consider both the spiral and a decaying spot localized at the spiral's outer end (radial location and azimuth of the spot are thus determined by the

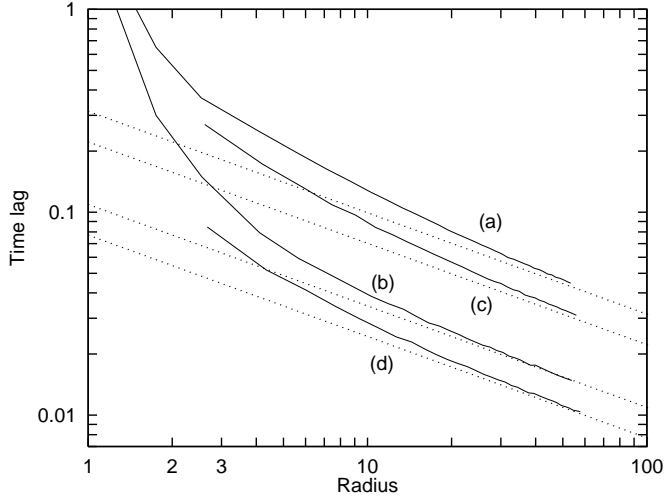


Fig. 2. Maximum time lag  $t_m$  shown between the rays from a ring of given radius in the Kerr metric (solid curves). Four cases are plotted for radii greater than  $r_{ms}$  and different combinations with the black-hole rotation parameter,  $a$ . The observer inclination angle  $\iota_0$  is: (a)  $a = 1$ ,  $\iota_0 = 80^\circ$ ; (b)  $a = 1$ ,  $\iota_0 = 20^\circ$ ; (c)  $a = 0$ ,  $\iota_0 = 80^\circ$ ; (d)  $a = 0$ ,  $\iota_0 = 20^\circ$ . Radius is given in units of  $r_g$ , while the time lag is expressed with respect to Keplerian orbital period,  $t_k$ . The Euclidean estimate of  $t_m$  is also shown (dotted lines).

spiral's shape and its orientation with respect to the observer). Such a spot can represent a temporary  $\phi$ -axis are (its maximum amplitude  $A_m$  is a free parameter). See figure 1 for a general scheme of the model.

The complexities of primary X-ray reprocessing are overpassed by directly parametrizing the emissivity. Our approach to the emissivity parametrization is close to the computations of Sanbuichiet al. (1994) and Bao and Wita (1999), who considered a non-rotating black hole.

The spiral pattern is characterized by the emissivity distribution in the equatorial plane,

$$j_e^{(s)}(r; r_e; \iota_e) = j_0(r_0) r_e^{-\alpha} \sin \iota_e(r_e); \quad (1)$$

where the frequency-dependent term,  $j_0$ , is taken as a narrow Gaussian profile, while the power-law index,  $\alpha$ , describes the overall radial decrease in the emissivity. The spiral rotates with respect to the observer, and its shape is logarithmic and determined by the function  $\iota_e(r) = \iota_0 + \arctan \log(r/r_0)$ , where  $\arctan$  is the pitch angle, and  $r_0$  is the outer radius where the wave is being excited.<sup>2</sup> This parametrization approximates the spiral

pattern evolving on the background of a Keplerian disc. The azimuthal form of the spiral depends also on the type of perturbation, so what we use here is one of the possible modes, which appears to be simple enough for illustration purposes.

As already discussed, the model takes inspiration from spirals in close binaries where a spot arises following the interaction between the stream (after the Roche-lobe overflow) and the disc (e.g., Wolf et al. 1998). The radiation flux in the spot decays with an  $e$ -folding time of  $q > 1$  orbital periods,  $t_k = 2\pi(r_e^3 + a)$ . A gain, the frequency-dependent part,  $j_0$ , of the spot intrinsic profile is taken in the Gaussian form and is assumed to be sufficiently narrow (its smearing is due mainly to radial component of the source orbital motion), while the amplitude,  $A(r; \iota_e)$ , decreases exponentially with the distance from the arc center located at  $r_0$ ,

$$j_e^{(f)}(r; r_e; \iota_e) = j_0(r_0) A(r_e; \iota_e) t^{-q}; \quad (2)$$

Here,  $A(r; \iota_e) = A_m \exp(-r/r_0)$  with, typically, the spot size  $r = |r - r_0|/r_0 < 1$  and  $r_0 > 20$ . Hence, the resulting emissivity is a sum of contributions (1) and (2):  $j_e = j_e^{(s)} + j_e^{(f)}$ .

It is the exact form of the emissivity distribution along the disc surface which determines the observed flux in the line wings and, in particular, which of the two wings | the bluish or the reddish one, appears more pronounced in the predicted spectrum. Thereby the lines are more complex than one would expect on the basis of intuition with simple ring-type sources (double-horn profiles). Here, we assume that a spiral with two arms extends from  $r = r_0$  down to  $r_{ms}$ , being terminated at the innermost stable orbit. Single-armed spirals show comparable spectral characteristics, but their variations occur with a double period and a somewhat higher amplitude, similar to the case of an elongated spot.

### 2.3. Light-Travel Time Near a Black Hole

Now we concentrate our attention on the consequences of finite light-travel time upon line variations.

One can write an order-of-magnitude (Euclidean) estimate of the maximum light-travel time delay,  $t_m$ , of rays originating in an equatorial ring (radius  $r_e$  centered on the black hole):  $t_m(r_e; \iota_0) \approx r_e^{1-2} \sin \iota_0$  ( $\iota_0$  is the observer's inclination). Here,  $t_m$  characterizes the mutual delay of the signals emitted at different parts of the ring, and is defined as the span in arrival times of the rays originating at different  $\iota_e$ .<sup>3</sup> Usually,  $r_e$  is sup-

2 The locally emitted intensity (denoted by subscript "e") is related to the observed intensity at spatial infinity (subscript "o") by the formula  $j_e(r_e; t) = j_o(r_o; t) = j_o(r_o; t) / g_{00}$ ; where the ratio  $g_{00} = e^{\phi}$  defines the redshift factor and  $t = t(r_e; \iota_e; a)$  is time delay due to the light-travel time along the ray. See Fanton et al. (1997) and Martocchia, Karas and Matt (2000) for further details on ray-tracing computations.

3 Light rays were approximated as straight lines for the purpose of estimating  $t_m$  here. For consistency with subsequent paragraphs, the standard notation will be adopted for Kerr spacetime in Boyer-Lindquist coordinates (Misner et al. 1973). Geometrized units  $c = G = 1$  are used and all lengths are made dimensionless by expressing them in units of the typical mass of the central black hole,  $M = 10^7 M_\odot$ .

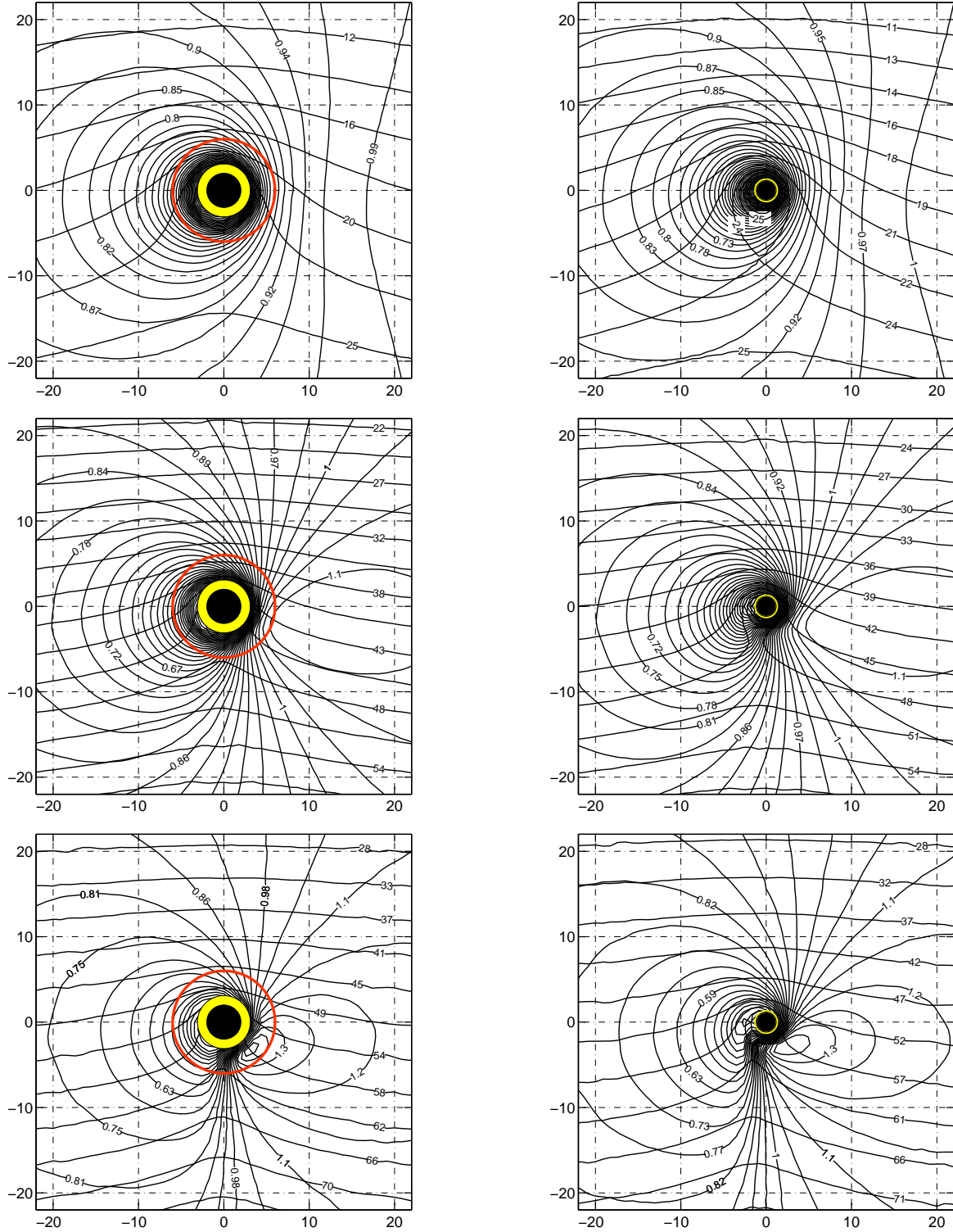


Fig. 3. Isocontours of constant light-travel time  $t$  and of redshift function  $g$  are shown in equatorial plane of the Kerr black hole. The contours are shown for a non-rotating black hole ( $a = 0$ , left panels), and for a maximally rotating hole ( $a = 1$ , right panels). Observer inclination is, from top to bottom,  $i_o = 20^\circ$ ,  $i_o = 50^\circ$ , and  $i_o = 80^\circ$ . For  $a = 0$ , three circles are plotted with radii of the horizon, of the circular photon orbit, and of the marginally stable orbit. The circles coincide with each other if  $a = 1$  (corotating orbits are assumed).

posed to be greater than a marginally stable orbit,  $r_{ms}$ :  $r_{ms} = 3r_g$  for a non-rotating black hole with  $a = 0$ ; and  $r_{ms} \rightarrow r_g$  for a maximally rotating black hole,  $a \rightarrow 1$  ( $r_g = 1 + \frac{1}{a^2}$ ). Light-travel time can be ignored provided  $t_{\text{in}} \rightarrow 1$ . On the other hand, the lags become increasingly important when the radiation source extends very close to the black-hole horizon where the resulting situation is further complicated by the lensing effect.

The geometrical time lag can be roughly characterized by  $t_{\text{in}}$ , which indicates whether the Euclidean formula estimates the correct value of the light-travel time with an acceptable precision, or whether relativistic effects modify the actual delays significantly. Figure 2 gives  $t_{\text{in}}$  for a source located at  $r_e = r_{ms}$ . The solid curves represent the values of the delay computed in Kerr spacetime, while the dotted lines (slope  $\sim 2$ ) show the approximation. Relativistic corrections become increasingly important for  $r_e = r_g < 3$ , in which case  $t_{\text{in}}$  increases sharply. On the other hand, the difference between the exact value of  $t_{\text{in}}$  and its Euclidean approximation is less than 10% for a source location  $> 5r_g$ .

Figure 3 shows the absolute value of light-travel time difference  $\Delta t$  between a reference ray (arbitrarily chosen but fixed) and a ray coming from a given point of emission  $r_e, \theta_e$  in the equatorial plane ( $\phi = 90^\circ$ ). In this figure,  $\Delta t$  was calculated in Kerr metric (no approximation was used here). Given  $a$  and  $\phi_o$ , the values of  $\Delta t$  determine where in the disc the corrections on the time lag play an important role. Reference values of  $\Delta t$  can be transformed to physical units, as measured by a distant observer, by the relation  $\Delta t[\text{s}] = 10M_7 \Delta t$ . The equatorial plane is portrayed from above (along the common rotation axis of the hole and of the disc), and a distant observer is located at the top (Cartesian  $y \rightarrow 1$ ; coordinates  $x$  and  $y$  are introduced in the disc plane by  $x^2 + y^2 = r_e^2$ ). Contours of constant time lag are almost horizontal far from the hole. A distortion of the contours from straight lines occurs near to the hole due to a lensing effect and gravitational delay. (Indeed, the contour lines can even become split into two disjoint parts.) Next, the redshift function,  $g$ , is also plotted by another set of contour lines in figure 3. Relativistic effects on the time lag and redshift are more important for a maximally rotating black hole (right panels) because of the smaller  $r_{ms}$ .

#### 2.4. Parameters of Spiral-Wave Line Profiles

Spiral-wave structures produce a rich variety of spectra and light curves, much broader than we can observe in the case of localized spots. Apart from the black hole angular momentum,  $a$ , and the orientation angle of the source with respect to observer,  $\phi_o$ , one can identify several parameters related to the geometry and orbital motion of such spirals which determine the spectral variability:

ity:

The non-axisymmetric intrinsic emissivity of the source is described by equation (1) with free parameters  $(\phi_o, \phi, r_0)$  determining the azimuthal and radial dependence of emissivity.

Doppler shifts between the emitted and detected radiation increase the centroid energy and intensity of the rays originating at the approaching side of the source, and vice versa for the receding side (factor  $g^3$ ). This effect tends to enlarge the width of the spectral features and to enhance the observed flux at its high-energy tail.

Gravitational redshift affects mainly photons coming from the inner parts of the source. This effect decreases the centroid energy of the line.

Light-travel time determines, along with the shape of the spiral, which photons are received at the same instant of time. We remark that contours of constant time delay are deformed near the hole. Hence, variability amplitude can be much accentuated if the spiral coincides with one of the contours at certain orbital phase. This effect influences the flux from some patterns under suitable orientation.

Gravitational lensing enhances the flux from the far side of the source (the part of the source which is at the upper conjunction with the hole). This tends to increase the observed flux around the centroid energy.

All parameters of the intrinsic emissivity and of the black hole spacetime enter in computations of the individual ray trajectories which form the resulting radiation flux at the detector. We find that the dependence of observed profiles on  $\phi_o$  is rather weak for a typical choice of  $0 < \phi_o < 2$ . One should be aware of other implicit parameters which were kept fixed in the present model: the inner radius of the spiral pattern (here  $r_{ms}$ ), the (small) width of the intrinsic Gaussian local line profile, the number of spiral patterns (here  $n = 2$ ), and duration of the flare ( $> t_k$ ). In all of these computations, for the sake of simplicity the radiation was emitted isotropically in the rest frame of the gaseous medium.

### 3. Results

A typical line profile of a double-armed spiral is shown in figure 4 where the observed spectral feature is plotted as a function of the observed energy and orbital phase. The variation in the spectrum is shown over the whole revolution of the pattern by 2 in azimuth (as the normalized phase ranges from 0 to 1), while energy axis is normalized to the local emission energy,  $E_e$ . Contours of the dynamical spectrum are shown by projecting the surface plot onto the plane of energy vs. phase. Here, one can clearly identify that the contribution of the spiral alone is repeated twice in each of the subplots (because we considered double arms), but the total signal does not bear this property because of the decaying flare contribution. Next, figures 5{6 show these contours for different model parameters. The contours are plotted with uni-

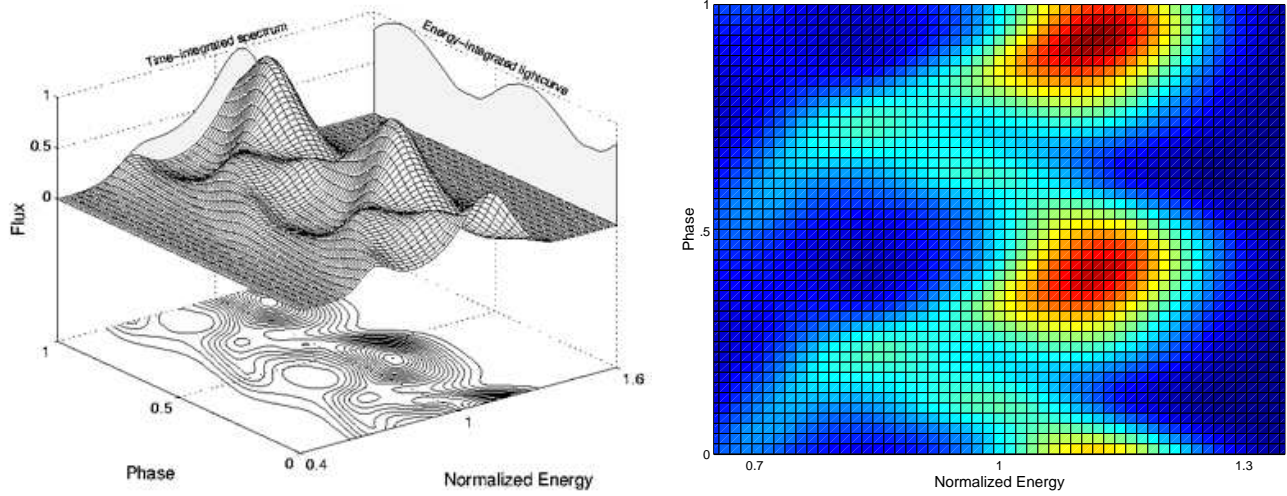


Fig. 4. Example of the dynamical spectrum of a line from a spiral wave near a black hole ( $a = 0$ ). Left panel: The predicted flux is background subtracted and normalized to maximum. The energy-integrated lightcurve and time-integrated spectrum are also shown. The parameters for this plot were  $\beta = 6$ ,  $\beta = 18$ ,  $\alpha = 0$ ,  $r_0 = 13$ ,  $A_m = 1$ . The inclination angle was kept fixed at  $5^\circ$ . Right panel: Projection is shown onto normalized energy vs. phase diagram with flux indicated by different levels of shading.

form spacings between the maximum flux and zero flux of the signal from which the underlying continuum is subtracted.

### 3.1. The Predicted Form of Observed Profiles

The parameter space has been explored systematically in the following manner.

Black-hole angular momentum:  $a = 0$  (columns denoted by letters a, c, e, g), and  $a = 1$  (b, d, f, h). The two cases correspond to a non-rotating and to maximally rotating hole, respectively.

Observer inclination:  $\alpha = 20^\circ$  (the rows denoted by roman numbers i{iii}),  $\alpha = 50^\circ$  (iv{vi}), and  $\alpha = 80^\circ$  (vii{ix}). The disc plane is  $\alpha = 90^\circ$ .

The outer edge of the spiral pattern:  $r_0 = 7$  (i, iv, vii),  $r_0 = 13$  (ii, v, viii), and  $r_0 = 20$  (iii, vi, ix). Units of  $GM = c^2$  are used.

The form of spiral pattern, as defined by its pitch angle  $\arctan p$  and contrast in eq. (1):  $\beta = 3$ ,  $\beta = 8$  (a, b);  $\beta = \sqrt{3}$ ,  $\beta = 8$  (c, d);  $\beta = 6$ ,  $\beta = 8$  (e, f);  $\beta = 6$ ,  $\beta = 18$  (g, h). Large values of  $\beta$  correspond to well-defined spirals (with small width and large contrast), while large values of  $\beta$  denote tightly wound spirals (corresponding to high Mach number in the disc medium).

A contribution of the  $\beta$  are to the line in terms of its duration parameter,  $q = 2$  (units of the orbital period), and the initial flux,  $A_m$ . The average ratio of the  $\beta$ -to-spiral intrinsic emissivity in the centre of the line was taken as  $A_m = 1:2^4$  for a weak  $\beta$  (figure 5) and  $A_m = 1:1$  for a strong one (figure 6).

In each of the sub-figures the spectra were computed with sufficient resolution in energy and phase ( $10^{-2}$ – $10^2$

grid) by the ray-tracing code (Martocchia 2000).

One can recognize several characteristic features of the dynamical spectra. The  $\beta$  are is easily distinguished in figure 6 where it was assumed to be more intense with respect to the spiral pattern than in figure 5. However, even in the latter situation the Doppler boosted radiation of the  $\beta$  are dominates over the extended spiral when the disc is viewed at large inclination, and especially if the whole source is near to the horizon ( $r_0 \approx 7$ ; see the row vii). Next, one can recognize the effect of gravitational redshift if the source is seen almost along the rotation axis (i{iii}), whereas this effect turns out to be less visible in very broad spectral features corresponding to large inclinations (vii{ix}).

### 3.2. The Case of MCG 6{30{15

While the two plates in figures 5{6 has given us a general feeling for the influence of different parameters, a suitable ( $\chi^2$  minimizing) routine is used in practice for fitting the computed profiles to data.

Figure 7 shows the best fits to three iron-line profiles in MCG 6{30{15 (we use exactly the same data as defined by Iwasawa et al. 1996). These correspond to the spectral states of the source during its 1994 observation with the ASCA satellite. Here, we do not intend to exactly mimic what is going on in the source, because this appears to be premature with the available data. It is, however, possible to constrain the distance from the centre at which the line could originate, depending on the angular momentum of the hole and inclination of the observer.

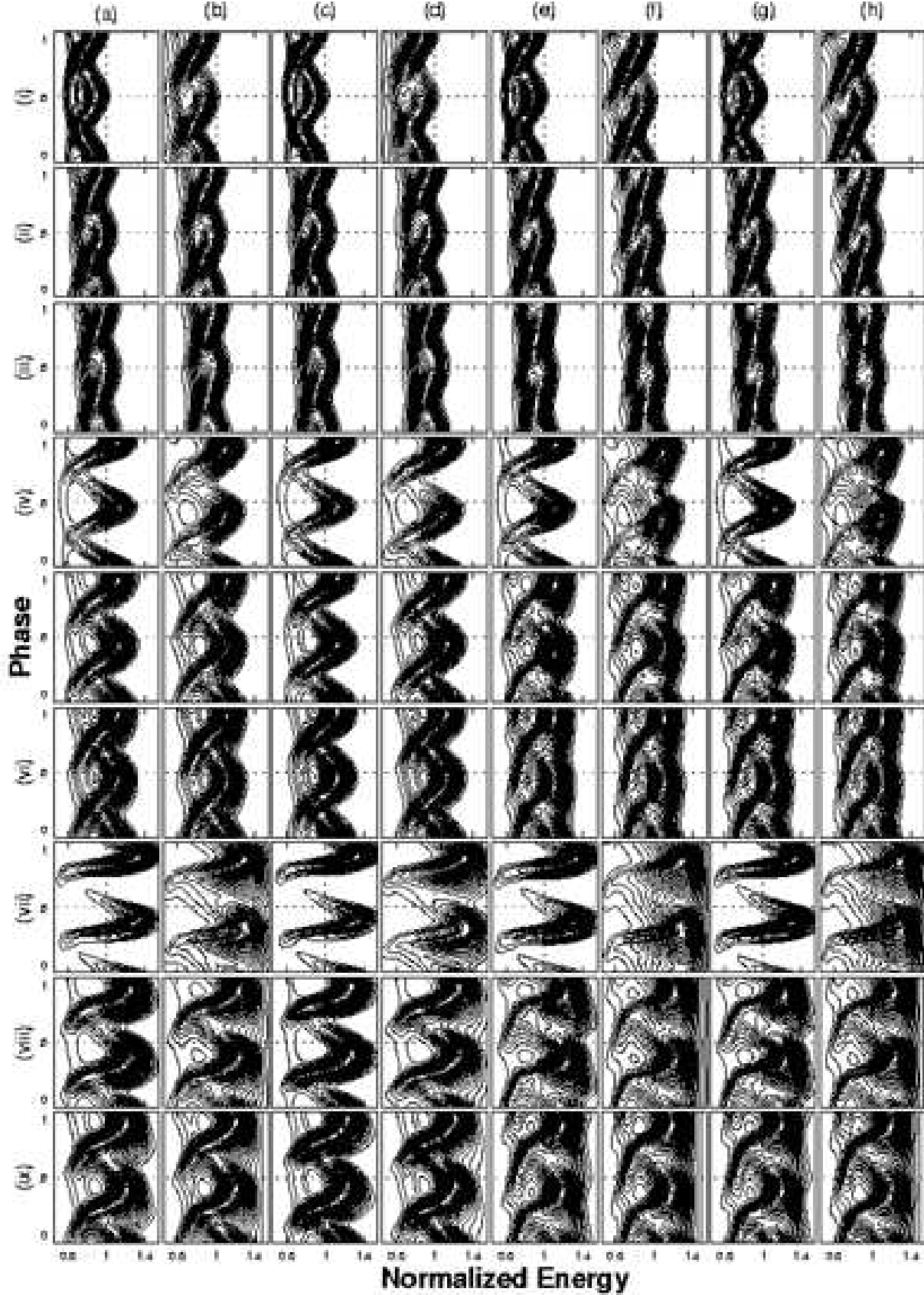


Fig. 5. Dynamical spectra of the two-arm pattern with a slowly decaying  $\alpha$  are. Different cases correspond to the form of the spiral, rotation parameter of the black hole, and observer's view angle (see the text for details). Here, the spiraldominates over the  $\alpha$  are.

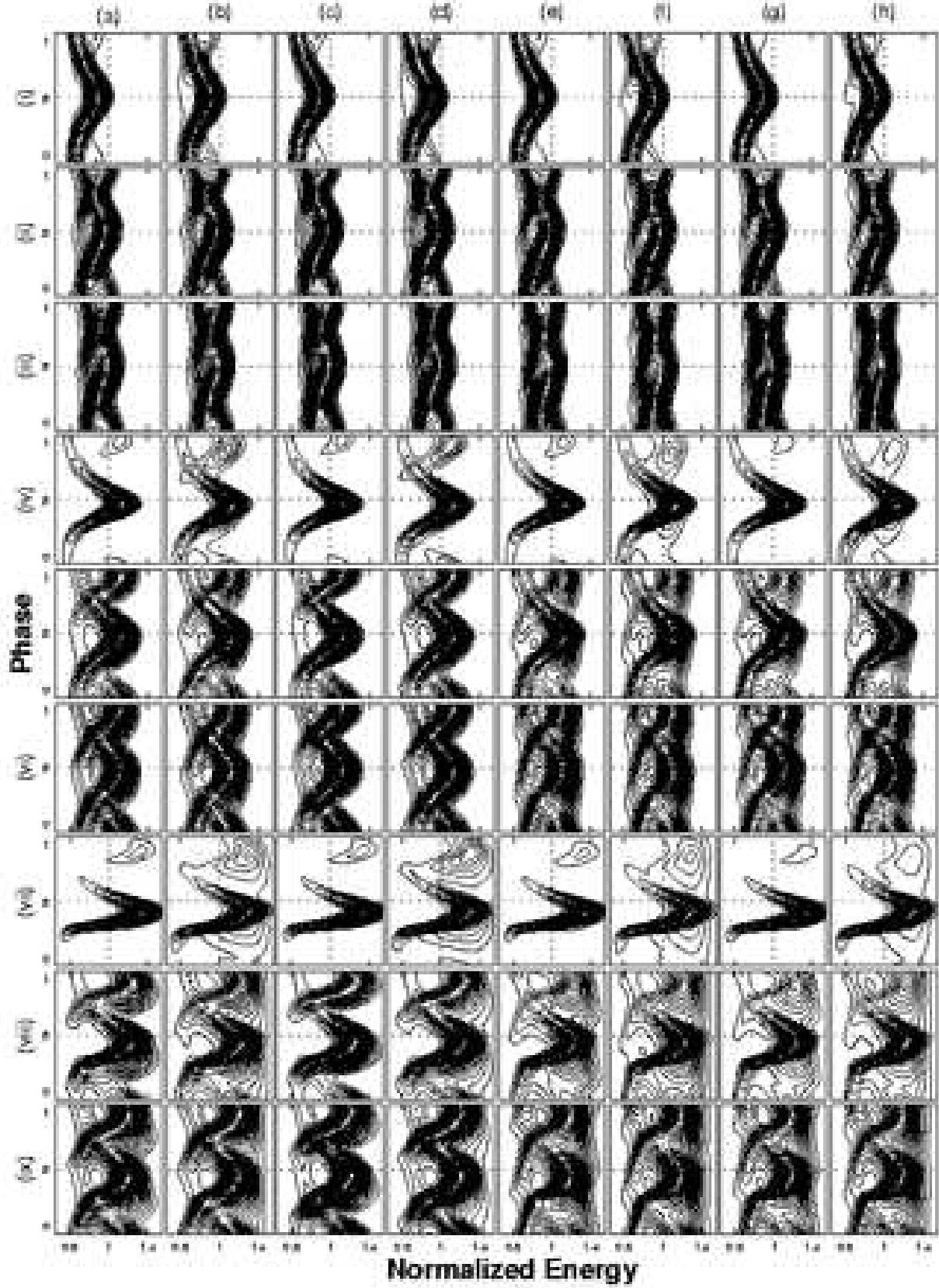


Fig. 6. Same as in figure 5, but now the  $\alpha$  is assumed to be more pronounced. This represents an intermediate situation between a pure spiral and the orbiting spot model.

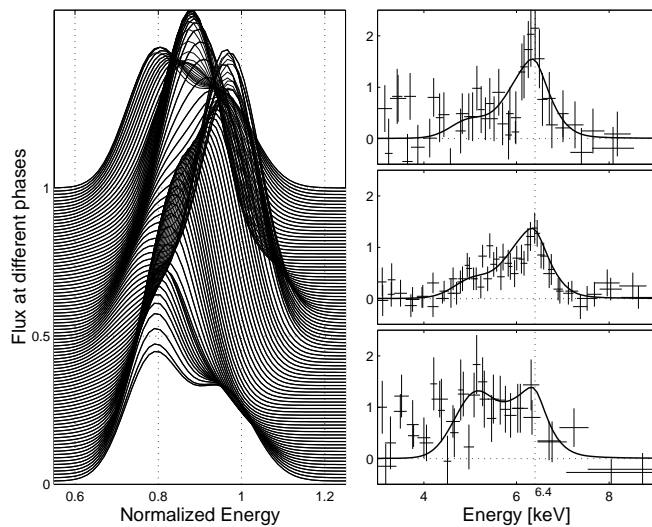


Fig. 7. Left: Time variation of the best-fit profile during the entire revolution of the spiral. Right: The computed profile is plotted after averaging to three different phases. The feature observed in MCG 6-30-15 (Iwasawa et al. 1996) is overlayed with an appropriate phase shift.

The curves shown in the right panels are those to which the  $\chi^2$  minimization routine converges in the parameter space (as described in subsection 3.1.). The reduced  $\chi^2$  is (from top to bottom):  $\chi^2_{\text{dof}} = 72/53, 40/55, 60/40$  for the three phases, respectively. Here,  $a = 0^\circ$ ,  $\phi_0 = 20^\circ$ ,  $r_0 = 13$ ,  $\alpha = 6^\circ$ ,  $\beta = 18^\circ$ ,  $A_m = 1/16$ . We thus find that the data are well fitted by the double arm at moderate inclination angles. In such a case, the dependence of the observed profile on  $a$  is negligible because a substantial part of the line flux originates sufficiently above  $r_{\text{ms}}$ .

#### 4. Discussion

In the present work we did not intend to elaborate the fits of MCG 6-30-15 data further. It is, however, worth noticing that even the adopted, rather simple scheme produces acceptable fits and the required, reddened line centroid also with small values of  $a$ . One can thus address the question if those redshifted and variable profiles of the iron line could be achieved without the necessity of invoking a large mass ( $> 10^7 M_\odot$ ) of the central object and/or its fast rotation, which have recently been put in certain doubt by several people. It is thus legitimate to consider all different viable options because various effects contribute to the line formation, and the interpretation of observed profiles is not straightforward.<sup>4</sup> A

self-consistent interpretation of the profiles cannot be achieved without regard to the underlying continuum component where it is crucial to distinguish between line and continuum photons.

Our discussion is relevant for X-ray variability of some spectral states observed in AGN and GBHCs; it is quite obvious, however, that only a part of the complex variability behaviour could be attributed to motion of large scale structures, such as spiral waves. The model is complementary to the discussion of inclination angles inducing the observed line variations, which enable one to restrict the geometry of the source by means of the reverberation technique. Proper evaluation of the light-travel time from different parts of the source is important in both schemes.

#### 5. Conclusions

We computed variable line profiles due to non-axisymmetric spiral-type patterns near a Kerr black hole. We adopted several simplifying assumptions and constrained some of the parameters to fixed values. Yet, we could show that a big variety of line profiles are reproduced and the data of MCG 6-30-15 which we used for illustration purposes can be modeled without the necessity of a  $\chi^2$ , although such a possibility is not rejected. Because the existence of spiral features is expected on the basis of theoretical models, our discussion seems to be better substantiated than data fitting by ad hoc functions. Also, the adopted approach uses computed profiles, rather than being restricted to integral quantities (centroid energy, line width, etc.); it can thus provide robust results once better-resolved data become available.

Our present scheme can be considered as complementary to the picture of Reynolds et al. (1999) and Ruszkowski (2000), who examined  $\phi$ -axis arcs above the disc surface as the origin of line variations, and to Vaughan and Edelson (2001), who addressed the problem of the link between line and continuum variations. Naturally, the phenomenological description of the source will have to be supplemented by a time-dependent physical model of X-ray reprocessing.

Although we applied our computations only to the case of MCG 6-30-15, there is a more general interest in the problem of spectral features from inner parts of gaseous discs endowed with spirals. Compact binaries with matter over flow represent another class of objects where our computations could be useful. Patterns like those discussed in this paper can be introduced in order to explain asymmetric lines and variability observed

<sup>4</sup> Weaver and Yaqoob (1998) and Reynolds and Begelman (1997) proposed alternative schemes which do not involve fast rotation of the black hole. Nowak and Chiang (2000) discussed the

possible caveats in interpretations of the present time-resolved spectra, and they concluded that the central mass is about  $10^6 M_\odot$ , much less than previously considered. A rather small mass, however, requires efficient emission, which also seems to pose a problem, so the issue has not been settled yet.

in UV/optical spectral bands from the broad-line region (Dumont, Collin-Souffrin 1990; Corbin 1997), and periodicities reported in the optical light curve of the blazar OJ287 (Takalo 1994; Villata et al. 1998). In these cases, however, the radiation is emitted at distances exceeding  $10^3$  gravitational radii, so that the general relativity calculations are unnecessary and the computations can be performed in a much faster way.

Even though the results cannot be conclusive with the present-day resolution, there is evident potentiality of this approach with planned missions, like Constellation-X and XEUS. The model of spirals illustrates the opportunity of tracing the surface structures on accretion discs.

We acknowledge support from the grants GACR 205/00/1685 and 202/99/0261. V.K. thanks for hospitality of the International School for Advanced Studies (Trieste) and Observatoire de Paris-Meudon.

## References

- Abramowicz, M. A., Bao, G., Lanza, A., & Zhang, X.-H. 1991, *A & A*, 245, 454
- Abramowicz, M. A., Lanza, A., Spiegel, E. A., & Szuszkiewicz, E. 1992, *Nature*, 356, 41
- Abrassart, A., & Czerny, B. 2000, *A & A*, 356, 475
- Adams, F. C., & Watkins, R. 1995, *ApJ*, 451, 314
- Bao, G., & Wiita, P. 1999, *ApJ*, 519, 80
- Blandford, R. D., & McKee, C. F. 1982, *ApJ*, 255, 419
- Chakrabarti, S. K., & Wiita, P. J. 1993, *A & A*, 271, 216
- Chakrabarti, S. K., & Wiita, P. J. 1994, *ApJ*, 434, 518
- Chen, K., & Hapem, J. P. 1990, *ApJ*, 354, L1
- Coppi, P. S. 1992, *MNRAS*, 258, 657
- Corbin, M. R. 1997, *ApJ*, 485, 517
- Done, C., & Nayakshin, S. 2001, *ApJ*, 546, 419
- Dumont, A.-M., & Collin-Souffrin, S. 1990, *A & A Suppl.*, 229, 313
- Dumont, A.-M., Abrassart, A., & Collin, S. 2000, *A & A*, 357, 823
- Eracleous, M. 1998, *Adv. Space Res.*, 21, 33
- Fabian, A. C., Iwasawa, K., Reynolds, C. S., & Young, A. J. 2000, *PASP*, 112, 1145
- Fanton, C., Calvani, M., de Felice, F., & Cadez, A. 1997, *PASJ*, 49, 159
- Galeev, A. A., Rosner, R., & Vaiana, G. S. 1979, *ApJ*, 229, 318
- Goldreich, P., & Tremaine, S. 1979, *ApJ*, 233, 857
- Haardt, F., Maraschi, L., & Ghisellini, G. 1994, *ApJ*, 432, L95
- Iwasawa, K., Fabian, A. C., Young, A. J., Inoue, H., & Matsumoto, C. 1999, *MNRAS*, 306, L19
- Iwasawa, K., Fabian, A. C., Reynolds, C. S., Nandra, K., Otani, C., Inoue, H., Hayashida, K., Brandt, W. N. et al. 1996, *MNRAS*, 282, 1038
- Karas, V. 1997, *MNRAS*, 288, 12
- Karas, V., Czerny, B., Abrassart, A., & Abramowicz, M. A. 2000, *MNRAS*, 318, 547
- Kato, S., Fukue, J., & Mineshige, S. 1998, *Black-Hole Accretion Discs* (Kyoto: Kyoto University Press)
- Kawaguchi, T., Mineshige, S., Machida, M., Matsumoto, R., & Shibata, K. 2000, *PASJ*, 52, L1
- Krolik, J. H. 1999, *Active Galactic Nuclei: From the Central Black Hole to the Galactic Environment* (Princeton: Princeton University Press)
- Kuo, C.-L., & Yuan, C. 1999, *ApJ*, 512, 79
- Lanzafame, G., Maravigna, F., & Belvedere, G. 2000, *PASJ*, 52, 515
- Lawrence, A., & Papadakis, I. 1993, *ApJ*, 414, L85
- Lee, E., & Goodman, J. 2000, *MNRAS*, 308, 984
- Malzac, J., & Jourdain, E. 2000, *A & A*, 359, 843
- Mangalam, A. V., & Wiita, P. J. 1993, *ApJ*, 406, 420
- Maoz, E., & McKee, C. F. 1998, *ApJ*, 494, 218
- Marsh, T. R., & Hame, K. 1988, *MNRAS*, 235, 269
- Martocchia, A. 2000, *X-ray Spectral Signatures of Accreting Black Holes*, Ph.D. Thesis, SISSA Trieste
- Martocchia, A., Karas, V., & Matt, G. 2000, *MNRAS*, 312, 817
- Martocchia, A., & Matt, G. 1996, *MNRAS*, 282, L53
- Misner, C. W., Thorne, K. S., & Wheeler, J. A. 1973, *Gravitation* (New York: W. H. Freeman and Co.)
- Mineshige, S., Ouchi, N. B., & Nishimori, H. 1994, *PASJ*, 46, 97
- Murray, J. R., Amisage, P. J., Ferrario, L., & Wickramasinghe, D. T. 1999, *MNRAS*, 302, 189
- Nayakshin, S. V. 1998, *Physics of Accretion Discs with Magnetic Flares*, Ph.D. Thesis, University of Arizona
- Nayakshin, S., Kazanas, D., & Kalman, T. R. 2000, *ApJ*, 537, 798
- Nowak, M. A., & Chiang, J. 2000, *ApJ*, 531, L13
- Rauch, K., & Blandford, R. D. 1994, *ApJ*, 421, 46
- Reynolds, C. S., & Begelman, M. C. 1997, *ApJ*, 488, 109
- Reynolds, C. S., Young, A. J., Begelman, M. C., & Fabian, A. C. 1999, *ApJ*, 514, 164
- Rickett, B. J., Coles, W. A., & Bourgois, G. 1984, *A & A*, 134, 390
- Rozyczka, M., & Spruit, H. C. 1993, *ApJ*, 417, 677
- Ruszkowski, M. 2000, *MNRAS*, 315, 1
- Sanbuchi, K., Fukue, J., & Kojima, Y. 1994, *PASJ*, 46, 605
- Sanders, R. H., & Huntley, J. M. 1976, *ApJ*, 209, 53
- Sawada, K., Matsuda, T., & Hachisu, I. 1986, *MNRAS*, 219, 75
- Steehls, D., & Stehle, R. 1999, *MNRAS*, 307, 99
- Tagger, M., Henriksen, R. N., Sygnet, J. F., & Pellat, R. 1990, *ApJ*, 353, 654
- Tagger, M., & Pellat, R. 1999, *A & A*, 349, 1003
- Takalo, L. 1994, *Vistas Astron.*, 38, 77
- Taylor, J. A. 1996, *ApJ*, 470, 269
- Ulrich, M.-H., Maraschi, L., & Urry, C. M. 1997, *ARA & A*, 35, 445
- Vaughan, S., & Edelson, R. 2001, *ApJ*, preprint
- Villata, M., Raiteri, C. M., Sillanpaa, A., & Takalo, L. O. 1998, *MNRAS*, 293, L13
- Wada, K. 1994, *PASJ*, 46, 165
- Weaver, K. A., & Yaqoob, T. 1998, *ApJ*, 502, L139
- Wolf, S., Barwig, H., Bobinger, A., Mantel, K.-H., & Sinic, D. 1998, *A & A*, 332, 984
- Yonehara, A., Mineshige, S., & Welsh, W. F. 1997, *ApJ*, 486, 388